

# Trapped proton fluxes at low Earth orbits measured by the PAMELA experiment

O. Adriani<sup>1,2</sup>, G. C. Barbarino<sup>3,4</sup>, G. A. Bazilevskaya<sup>5</sup>, R. Bellotti<sup>6,7</sup>, M. Boezio<sup>8</sup>,  
E. A. Bogomolov<sup>9</sup>, M. Bongi<sup>1,2</sup>, V. Bonvicini<sup>8</sup>, S. Bottai<sup>2</sup>, A. Bruno<sup>6,\*</sup>, F. Cafagna<sup>7</sup>,  
D. Campana<sup>4</sup>, R. Carbone<sup>8</sup>, P. Carlson<sup>10</sup>, M. Casolino<sup>11,12</sup>, G. Castellini<sup>13</sup>,  
I. A. Danilchenko<sup>14</sup>, C. De Donato<sup>11,15</sup>, C. De Santis<sup>11,15</sup>, N. De Simone<sup>11</sup>, V. Di Felice<sup>11,16</sup>,  
V. Formato<sup>8,17</sup>, A. M. Galper<sup>14</sup>, A. V. Karelin<sup>14</sup>, S. V. Koldashov<sup>14</sup>, S. Koldobskiy<sup>14</sup>,  
S. Y. Krutkov<sup>9</sup>, A. N. Kvashnin<sup>5</sup>, A. Leonov<sup>14</sup>, V. Malakhov<sup>14</sup>, L. Marcelli<sup>11,15</sup>,  
M. Martucci<sup>15,18</sup>, A. G. Mayorov<sup>14</sup>, W. Menn<sup>19</sup>, M. Mergé<sup>11,15</sup>, V. V. Mikhailov<sup>14</sup>,  
E. Mocchiutti<sup>8</sup>, A. Monaco<sup>6,7</sup>, N. Mori<sup>1,2</sup>, R. Munini<sup>8,17</sup>, G. Osteria<sup>4</sup>, F. Palma<sup>11,15</sup>,  
B. Panico<sup>4</sup>, P. Papini<sup>2</sup>, M. Pearce<sup>10</sup>, P. Picozza<sup>11,15</sup>, M. Ricci<sup>18</sup>, S. B. Ricciarini<sup>2,13</sup>,  
R. Sarkar<sup>20,21</sup>, V. Scotti<sup>3,4</sup>, M. Simon<sup>19</sup>, R. Sparvoli<sup>11,15</sup>, P. Spillantini<sup>1,2</sup>, Y. I. Stozhkov<sup>5</sup>,  
A. Vacchi<sup>8</sup>, E. Vannuccini<sup>2</sup>, G. I. Vasilyev<sup>9</sup>, S. A. Voronov<sup>14</sup>, Y. T. Yurkin<sup>14</sup>, G. Zampa<sup>8</sup>,  
N. Zampa<sup>8</sup>, and V. G. Zverev<sup>14</sup>

<sup>1</sup> Department of Physics and Astronomy, University of Florence, I-50019 Sesto Fiorentino,  
Florence, Italy

<sup>2</sup> INFN, Sezione di Florence, I-50019 Sesto Fiorentino, Florence, Italy

<sup>3</sup> Department of Physics, University of Naples “Federico II”, I-80126 Naples, Italy

<sup>4</sup> INFN, Sezione di Naples, I-80126 Naples, Italy

<sup>5</sup> Lebedev Physical Institute, RU-119991 Moscow, Russia

<sup>6</sup> Department of Physics, University of Bari, I-70126 Bari, Italy

<sup>7</sup> INFN, Sezione di Bari, I-70126 Bari, Italy

<sup>8</sup> INFN, Sezione di Trieste, I-34149 Trieste, Italy

<sup>9</sup> Ioffe Physical Technical Institute, RU-194021 St. Petersburg, Russia

<sup>10</sup> KTH, Department of Physics, and the Oskar Klein Centre for Cosmoparticle Physics,  
AlbaNova University Centre, SE-10691 Stockholm, Sweden

<sup>11</sup> INFN, Sezione di Rome “Tor Vergata”, I-00133 Rome, Italy

<sup>12</sup> RIKEN, Advanced Science Institute, Wako-shi, Saitama, Japan

<sup>13</sup> IFAC, I-50019 Sesto Fiorentino, Florence, Italy

<sup>14</sup> National Research Nuclear University MEPhI, RU-115409 Moscow, Russia

<sup>15</sup> Department of Physics, University of Rome “Tor Vergata”, I-00133 Rome, Italy

<sup>16</sup> Agenzia Spaziale Italiana (ASI) Science Data Center, Via del Politecnico snc, I-00133  
Rome, Italy

<sup>17</sup> Department of Physics, University of Trieste, I-34147 Trieste, Italy

<sup>18</sup> INFN, Laboratori Nazionali di Frascati, Via Enrico Fermi 40, I-00044 Frascati, Italy

<sup>19</sup> Department of Physics, Universitt Siegen, D-57068 Siegen, Germany

<sup>20</sup> Indian Centre for Space Physics, 43 Chalantika, Garia Station Road, Kolkata 700084,  
West Bengal, India

<sup>21</sup> Previously at INFN, Sezione di Trieste, I-34149 Trieste, Italy.

Received \_\_\_\_\_; accepted \_\_\_\_\_

---

\*Corresponding author. E-mail address: [alessandro.bruno@ba.infn.it](mailto:alessandro.bruno@ba.infn.it).

## ABSTRACT

We report an accurate measurement of the geomagnetically trapped proton fluxes for kinetic energy above  $\sim 70$  MeV performed by the PAMELA mission at low Earth orbits (350–610 km). Data were analyzed in the frame of the adiabatic theory of charged particle motion in the geomagnetic field. Flux properties were investigated in detail, providing a full characterization of the particle radiation in the South Atlantic Anomaly region, including locations, energy spectra and pitch angle distributions. PAMELA results significantly improve the description of the Earth’s radiation environment at low altitudes placing important constraints on the trapping and interaction processes, and can be used to validate current trapped particle radiation models.

*Subject headings:* astroparticle physics — atmospheric effects — cosmic rays — elementary particles — magnetic fields — space vehicles

## 1. Introduction

The radiation or Van Allen belts are regions of the Earth’s magnetosphere where energetic charged particles experience long-term magnetic trapping. The outer belt is predominately populated by electrons with hundreds of keV to MeV energies. The inner belt consists of an intense radiation of energetic protons (up to a few GeV), with a minor component of  $e^\pm$  and ions. Protons with energies greater than some tens of MeV are mainly originated from the  $\beta$ -decay of free neutrons produced in the interaction of galactic cosmic rays (CRs) with the Earth’s atmosphere, according to the so-called “Cosmic Ray Albedo Neutron Decay” (CRAND) mechanism (Singer 1958; Farley & Walt 1971).

The most widespread empirical trapped proton model in last decades is the NASA AP8 model (Sawyer & Vette 1976), a static global map of long-term average trapped proton flux, based on a series of measurements performed in the 1960s and early 1970s; two versions were developed, for maximum and minimum solar conditions respectively. Similar models were provided by the Institute of Nuclear Physics of Moscow State University (INP/MSU, Getselev et al. 1991). Recently, significant improvements (Meffert & Gussenhoven 1994; Huston & Pfitzer 1998; Heynderickx et al. 1999; Xapsos et al. 2002) have been made thanks to the data from new satellite experiments, such as CRRES (Gussenhoven et al. 1993, 1995), SAMPEX/PET (Looper et al. 1996, 1998) and the TIROS/NOAA series (Huston et al. 1996). Nevertheless, the modeling of the low altitude radiation environment is still incomplete, with largest uncertainties affecting the high energy ( $> 50$  MeV) fluxes in the inner zone and the South Atlantic Anomaly (SAA), where the inner belt makes its closest approach to the Earth’s surface<sup>1</sup>.

---

<sup>1</sup>The SAA is a consequence of the tilt ( $\sim 10$  deg) between the magnetic dipole axis of the Earth and its rotational axis, and of the offset ( $\sim 500$  km) between the dipole and the Earth centers. This region is characterized by extremely low intensity of geomagnetic field, with a

New accurate measurements of the high energy ( $\gtrsim 70$  MeV) CR radiation in Low Earth Orbits (LEO) have been reported by the PAMELA mission (Picozza et al. 2007). Thanks to the orbit and the high identification capabilities, PAMELA is able to provide detailed information about particle fluxes in different regions of the terrestrial magnetosphere, including energy spectra, spatial and angular distributions. In particular, the spacecraft passes through the SAA, allowing the observation of geomagnetically trapped particles from the inner Van Allen belt. For the first time PAMELA has revealed the existence of a significant component of trapped antiprotons in the inner belt (Adriani et al. 2011a). In this article we present the measurement of the trapped proton fluxes.

## 2. PAMELA data analysis

PAMELA is a space-based experiment designed for a precise measurement of the charged cosmic radiation in the kinetic energy range from some tens of MeV up to several hundreds of GeV. The Resurs-DK1 satellite, which hosts the apparatus, has a semi-polar (70 deg inclination) and elliptical (350÷610 km altitude) orbit. The spacecraft is 3-axis stabilized. The orientation is calculated by an onboard processor with an accuracy better than 1 deg which, together with the good angular resolution ( $< 2$  deg) of PAMELA, allows particle direction to be measured with high precision.

The analyzed data set includes protons acquired by PAMELA between July 2006 and September 2009. In order to account for the time variations of PAMELA detector performance, with the major effect related to the sudden failure of some front-end chips in the tracking system, data were divided into sub-sets; consistently with the spacecraft orbit precession rate, the sub-set width was chosen to be of about 244 days. Measured rigidities

---

significant contribution from non-dipolar components.

were corrected for the energy loss in the apparatus with MonteCarlo simulations. Details about apparatus performance, particle selection, efficiencies and measurement uncertainties can be found elsewhere (Adriani et al. 2011b, 2013).

Data were analyzed in the framework of the adiabatic theory, which provides a relatively simple description of the complex dynamics of charged particles in the magnetosphere. The motion of trapped particles was assumed to be as a superposition of three periodic motions: a gyration around the local magnetic field lines, a bouncing along field lines between conjugate mirror points in the northern and southern magnetic hemispheres, and a drift around the Earth. Each type of motion is related to an adiabatic invariant, which is conserved under the condition of small magnetic field variations during the period of the motion, and in absence of energy loss, nuclear scattering and radial diffusion (Walt 1994). In order to reject events near the local geomagnetic cutoff, characterized by chaotic trajectories of non-adiabatic type, only protons with rigidities  $R < 10/L^3$  GV were selected, where  $L$  is the McIlwain's parameter (McIlwain 1966) measured in Earth's radii ( $R_E=6371.2$  km).

McIlwain's coordinates and other variables of interest, as the adiabatic invariants, were calculated on an event-by-event basis using the IRBEM library (Boscher et al. 2012). The IGRF-10 (Macmillan & Maus 2010) and the TS05 (Tsyganenko & Sitnov 2005) models were used for the description of the internal and external geomagnetic field, respectively: the former employs a global spherical harmonic implementation of the main magnetic field; the latter is a dynamical (5-min resolution) model of the storm-time geomagnetic field in the inner magnetosphere, based on recent satellite measurements.

## 2.1. Trajectory reconstruction

Proton trajectories were reconstructed in the Earth’s magnetosphere using a tracing program based on numerical integration methods (Smart & Shea 2000, 2005), and implementing the afore-mentioned geomagnetic field models. For each event, the number of gyrations, bounces and drifts was evaluated in order to estimate corresponding frequencies and check trajectory behaviors. Trajectories were propagated back and forth from the measurement location, and traced until:

1. they reached the model magnetosphere boundaries;
2. or they intersected the absorbing atmosphere limit, which was assumed at an altitude<sup>2</sup> of 40 km;
3. or they performed more than  $10^6/R^2$  steps, where  $R$  is the particle rigidity in GV, for both propagation directions.

The first case (1) corresponds to protons from interplanetary space possibly surviving the cutoff selection  $R < 10/L^3$ , which were excluded from the analysis. Events satisfying the last condition (3) were classified as stably-trapped protons: since the program uses a dynamic variable step length, which is of the order of 1% of a particle gyro-distance in the magnetic field, the applied rigidity-dependent criterion ensures that at least 4 drift cycles around the Earth were performed. Their trajectories were verified to fulfil the adiabatic conditions, in particular the hierarchy of temporal scales:

$$\omega_{gyro} \gg \omega_{bounce} \gg \omega_{drift}, \tag{1}$$

---

<sup>2</sup>Such a value approximately corresponds to the altitude where the most of CR interactions on atmosphere takes place.

where  $\omega_{gyro}$ ,  $\omega_{bounce}$  and  $\omega_{drift}$  are the frequencies associated to the gyration, the bouncing and the drift motion, respectively; estimated frequency ratios  $\omega_{bounce}/\omega_{gyro}$  and  $\omega_{drift}/\omega_{bounce}$  are of the order of  $10^{-2} \div 10^{-1}$ . Finally, the second category (2) includes quasi-trapped and un-trapped protons with limited lifetimes: the former have trajectories similar to those of stably-trapped protons, but are originated and re-absorbed by the atmosphere during a time larger than a bounce period (up to several tens of s); conversely, the latter precipitate into the atmosphere within a bounce period ( $\lesssim 1$ s). The analysis of such components is beyond the aim of this work and it will be the subject of a specific paper.

The trajectory analysis allows a deeper investigation of proton populations in LEO, including energy-dependent effects such as the breakdown of the trapping mechanism at high energies as consequence of either large gyro-radius or non-adiabatic trajectory effects (Selesnick et al. 2007).

## 2.2. Flux calculation

The factor of proportionality between fluxes and numbers of detected particles, corrected for selection efficiencies and acquisition time, is by definition the apparatus gathering power  $\Gamma$ . For an isotropic particle flux, the gathering power depends only on the detector design, and it is usually called the geometrical factor  $G_F$ . In the case of the PAMELA apparatus  $\Gamma$  (and  $G_F$ ) also depends on particle rigidity, due to the spectrometer bending effect on particle trajectories. Differently, in presence of anisotropic fluxes, the gathering power depends on the direction of observation as well. Consequently, an accurate estimate of  $\Gamma$  is crucial in evaluating fluxes inside and near the SAA region, where the trapped radiation is highly anisotropic as a consequence of the interaction with the Earth's atmosphere.



Similarly to Selesnick et al. (1995), the PAMELA effective area ( $\text{cm}^2$ ) was evaluated as a function of particle energy  $E_k$ , local pitch angle  $\alpha$  (i.e the angle between particle velocity vector and geomagnetic field line) and satellite orientation  $\Psi$  with respect to the geomagnetic field:

$$H(E_k, \alpha, \Psi) = \frac{1}{2\pi} \int_0^{2\pi} d\beta [A(E_k, \theta, \phi) \cdot \sin\alpha \cdot \cos\theta], \quad (2)$$

where  $\beta$  is the gyro-phase angle, and  $\theta=\theta(\alpha, \beta, \Psi)$  and  $\phi=\phi(\alpha, \beta, \Psi)$  are respectively the zenith and the azimuth angle describing particle direction in the PAMELA frame<sup>3</sup>, and  $A(E_k, \theta, \phi)$  is the apparatus response function (Sullivan 1971). For isotropic fluxes  $H$  does not depend on  $\Psi$  and it is related to the geometrical factor  $G_F(E_k)$  by:

$$G_F(E_k) = 2\pi \int_0^\pi d\alpha H(E_k, \alpha). \quad (3)$$

The effective area of the PAMELA apparatus was evaluated with Monte Carlo integration methods (Sullivan 1971), averaging it over  $\beta$  angle. The calculation was performed by varying  $\alpha$  in steps of 1 deg in the range  $0 \div 180$  deg. The satellite orientation  $\Psi = (\theta_\Psi, \phi_\Psi)$ , where  $\theta_\Psi$  and  $\phi_\Psi$  denote respectively the zenith and the azimuth angles<sup>4</sup> of geomagnetic field direction in the PAMELA reference frame, was varied in steps of  $\Delta\theta_\Psi, \Delta\phi_\Psi=1$  deg over the  $\Psi$  domain covered by the spacecraft. The dependency of the instrument response on proton energy was studied by estimating the effective area in 40 logarithmic bins ( $E_k = 63 \text{ MeV} \div 40 \text{ GeV}$ ).

---

<sup>3</sup>The PAMELA reference system has the origin in the center of the spectrometer cavity; the Z axis is directed along the main axis of the apparatus, toward the incoming particles; the Y axis is directed opposite to the main direction of the magnetic field inside the spectrometer; the X axis completes a right-handed system.

<sup>4</sup>Note that the PAMELA apparatus is not cylindrically symmetric.

In order to reduce statistical fluctuations due to the limited counts available in each  $(E_k, \alpha, \Psi)$  bin, a mean effective area was derived at each spacecraft geographic position  $\mathbf{X} = (Lat, Lon, Alt)$ :

$$H(\mathbf{X}, E_k, \alpha) = \frac{\sum_{\Psi \rightarrow \mathbf{X}} H(E_k, \alpha, \Psi) \cdot T(\Psi)}{\sum_{\Psi \rightarrow \mathbf{X}} T(\Psi)}, \quad (4)$$

by weighting each area contribution by the livetime spent by PAMELA at satellite orientations corresponding to  $\mathbf{X}$ .

Differential directional fluxes ( $GeV^{-1}m^{-2}sr^{-1}s^{-1}$ ) were calculated over a 5-dimensional grid  $F(\mathbf{X}, E_k, \alpha)$ :

$$F(\mathbf{X}, E_k, \alpha) = \frac{N(\mathbf{X}, E_k, \alpha)}{2\pi \cdot H(\mathbf{X}, E_k, \alpha) \cdot T(\mathbf{X}) \cdot \Delta\alpha \cdot \Delta E_k}, \quad (5)$$

where  $N(\mathbf{X}, E_k, \alpha)$  is the number of counts corrected for selection efficiencies, and  $T(\mathbf{X}) = \sum_{\Psi \rightarrow \mathbf{X}} T(\Psi)$  is the total livetime spent at  $\mathbf{X}$ . The flux grid extends over the whole phase-space region  $(\mathbf{X}, E_k, \alpha)$  covered by PAMELA, with  $\mathbf{X}$  resolution given by  $\Delta Lat, \Delta Lon = 2$  deg and  $\Delta Alt = 20$  km, for a total number of bins amounting to  $\sim 10^8$ .

### 2.3. East-West effect correction

Above several tens of MeV finite gyro-radius effects become not negligible. In particular, at PAMELA energies the proton gyro-radius can be large up to several hundreds of km, so that fluxes measured at a given position correspond to particles with different guiding center (i.e. the center of gyration) locations  $\mathbf{X}_{gc} = (Lat_{gc}, Lon_{gc}, Alt_{gc})$ . The atmospheric density averaged over a circle of gyration can be appreciably different from the density at the guiding center, the flux of protons arriving from East is lower than the one of protons from Western direction, since their guiding centers are located at lower altitudes and thus their flux is reduced by the atmospheric absorption. Such a phenomenon, known

as East-West effect (Lenchek & Singer 1962), was taken into account by evaluating fluxes at corresponding guiding center coordinates. However, the resulting correction is relatively small because of the limited apparatus aperture and since PAMELA major axis is mostly oriented towards the zenith direction.

## 2.4. Flux mapping

At a later stage, the geographic flux grid  $F(\mathbf{X}_{gc}, \alpha, E_k)$  was interpolated onto magnetic coordinates, using several invariant coordinate systems. In particular, distributions were evaluated as a function of adiabatic invariants, providing a convenient description of trapped fluxes. The versions of the adiabatic invariants used are:

$$M = \frac{p^2}{2m_0 B_m}, \quad (6)$$

$$K = \int_{s_m}^{s'_m} [B_m - B(s)]^{1/2} ds, \quad (7)$$

$$\Phi = \oint \mathbf{A} \cdot d\mathbf{l}, \quad (8)$$

where  $p$  is momentum,  $m_0$  is the proton rest mass,  $B$  is the local magnetic field,  $B_m$  is the mirror point magnetic field,  $s$  is distance along a magnetic field line, the integration is along the magnetic field between mirror point locations  $s_m$  and  $s'_m$ ,  $\mathbf{A}$  is the magnetic vector potential and the integration is along a curve which lies in the particle drift shell (Roederer 1970).  $M$ ,  $K$  and  $\Phi$  are related to the particle gyration, bounce and drift motion, respectively. It should be noted that the adiabatic invariants can not be treated as spatial coordinates since they are properties of the particles.

Alternatively, the particle energy  $E_k$  was used in place of  $M$ , and the Roederer parameter was used as drift invariant:

$$L^* = \frac{2\pi\mu E}{R_E\Phi}, \quad (9)$$

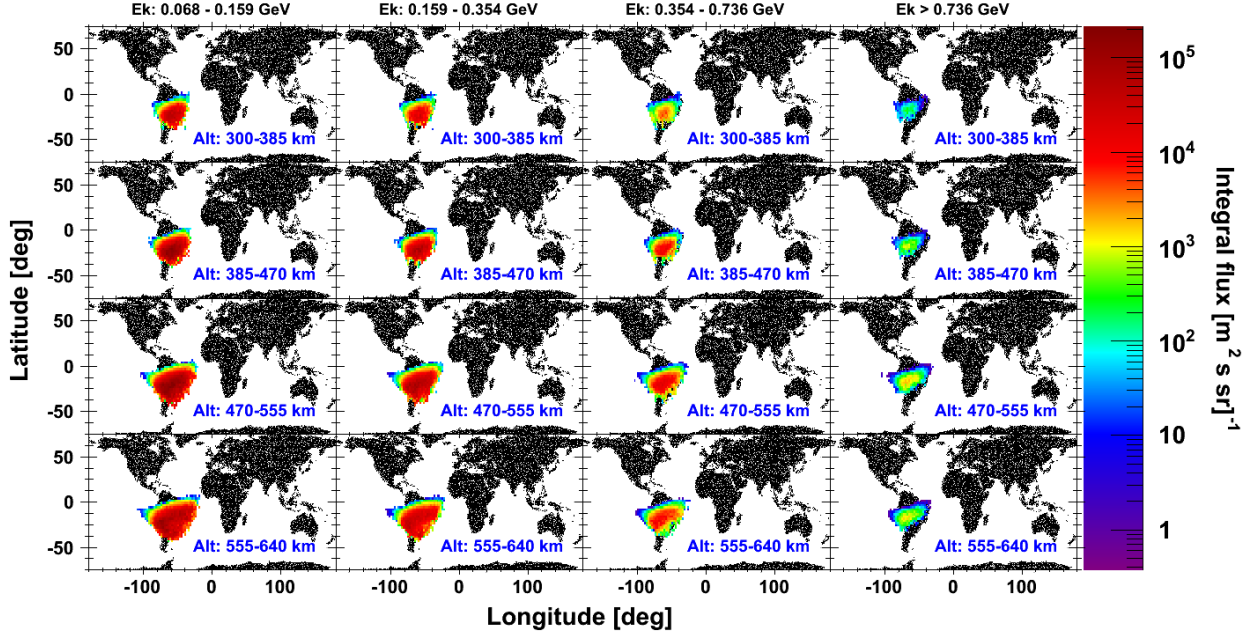


Fig. 1.— Stably-trapped integral fluxes ( $m^{-2}s^{-1}sr^{-1}$ ) averaged over the pitch angle range covered by PAMELA, as a function of geographic coordinates, evaluated for different energy (columns) and guiding center altitude (rows) bins.

where  $\mu_E$  is the Earth’s magnetic dipole moment (Roederer 1970). Note that, differently from  $\Phi$ , a constant dipole moment is necessary for  $L^*$  to be invariant due to secular geomagnetic variations: accordingly, PAMELA fluxes were calculated for the 1st Jan 2008.

Finally, in order to investigate the particle anisotropy, fluxes were also mapped as a function of equatorial pitch angle  $\alpha_{eq}$  and McIlwain’s  $L$ -shell. Such coordinates are commonly used in literature as bounce and drift invariants since they provide a more intuitive mapping, so they are useful for the comparison with other data sets.

### 3. Results

The selected sample amounts to  $\sim 9 \cdot 10^6$  events, including  $\sim 7.3 \cdot 10^6$  stably-trapped,  $\sim 5.4 \cdot 10^5$  quasi-trapped and  $\sim 1.2 \cdot 10^6$  un-trapped protons.

Geographic maps of the stably-trapped component are shown in Figure 1, for different bins of kinetic energy (columns) and guiding center altitude (rows). Fluxes were averaged over the local pitch angle range covered by PAMELA. Protons from the inner belt are detectable only in the SAA at such altitudes, spreading over a region located over South America. In particular, they concentrate in the South-East part of the SAA. The extension of covered area rapidly changes with altitude and energy. PAMELA is able to measure trapped fluxes up to their highest energies ( $\sim 4$  GeV).

Figure 2 shows the under-cutoff integral fluxes as a function of adiabatic invariants  $K$  and  $\Phi$  for different kinetic energy bins. In order to improve resolution,  $K^{1/2}$  and  $\log_{10}(\Phi)$  bins were used. The Y-axis ( $K = 0$ ) corresponds to the magnetic equator. Maps for the several populations (stably-, quasi- and un-trapped protons together with the whole under-cutoff proton sample) are reported. Similarly, Figure 3 shows fluxes as a function of equatorial pitch angle  $\alpha_{eq}$  and  $L$ -shell.

The first column in each figure reports results for stably-trapped protons. Constrained by the spacecraft orbit, the covered phase-space regions varies with the magnetic latitude. In particular, PAMELA can observe equatorial mirroring protons only for  $L$ -shell values up to  $\sim 1.18 R_E$  (or, equivalently, down to  $\Phi \sim 0.2 G \cdot R_E^2$ ), and measured distributions result in strips of limited width parallel to the “drift loss cone”, which delimits the  $\alpha_{eq}$  (or  $K$ ) range for which stable magnetic trapping does not occur. Fluxes exhibit high angular and radial dependencies.

For a comparison, the second and the third columns in Figures 2 and 3 show fluxes

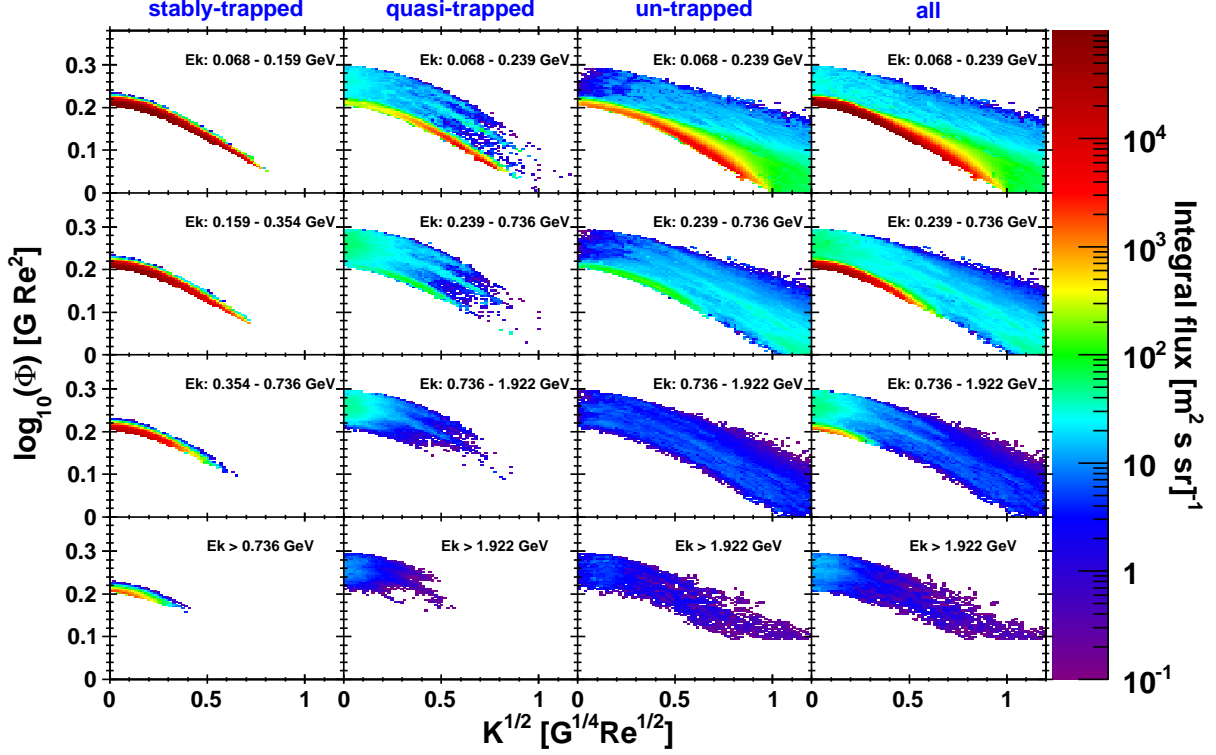


Fig. 2.— Proton integral fluxes ( $m^{-2}s^{-1}sr^{-1}$ ) as a function of the second  $K$  and the third  $\Phi$  adiabatic invariant, for different kinetic energy bins (see the labels). Results for the different populations are reported (from left to right): stably-trapped, quasi-trapped, un-trapped and the total under-cutoff proton sample.

for quasi- and un-trapped components. Measured maps result from the superposition of distributions corresponding to regions characterized by a different local (or bounce) loss cone value, i.e. the altitude of the mirror points changes with the longitude drift, decreasing from the SAA to the region on the opposite part of the planet (sometimes called “SouthEast-Asian Anomaly” or SEAA), the closest to the eccentric dipole center, where the geomagnetic field has a local maximum. Fluxes are quite isotropic, except for the SAA, where distributions are similar to those of stably-trapped protons; conversely, energy spectra outside the SAA are harder and extend to higher energies ( $\lesssim 7$  GeV), especially in

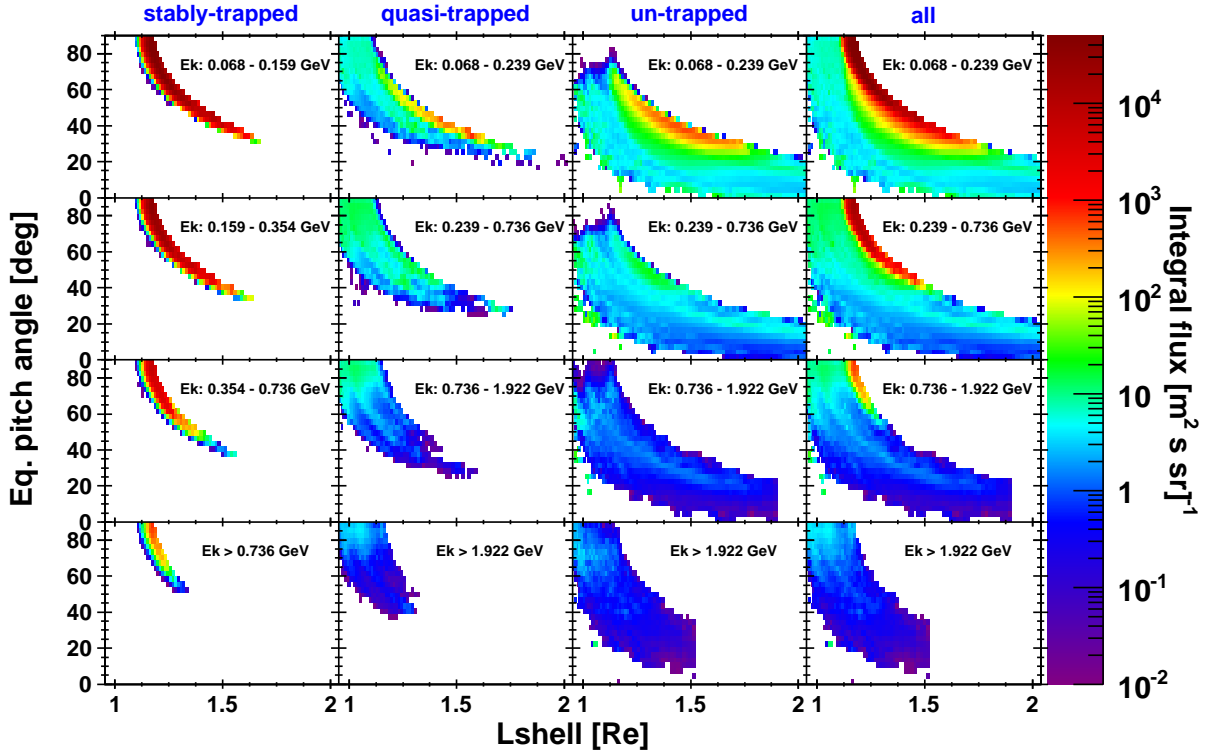


Fig. 3.— The same as Figure 2, but as a function of equatorial pitch angle  $\alpha_{eq}$  and McIlwain’s  $L$ -shell.

the SEAA, which is characterized by stronger trapping of energetic particles. Note that the un-trapped flux suppression at highest energy and  $L$  (or, equivalently, lowest  $\Phi$ ) bins is due to the used cutoff selection ( $R < 10/L^3$ ).

### 3.1. Comparison with models

Figure 4 compares PAMELA results and the predictions from two empirical models available in the same energy and altitude ranges. The former is the NASA AP8 model for solar minimum conditions, covering the energy range 0.1÷400 MeV (Sawyer & Vette 1976); originally based on omnidirectional maps, it was adapted for unidirectional fluxes

(UP8-min), and it implements the interpolation scheme by Daly & Evans (1996). The latter is the PSB97 model, based on data from the SAMPEX/PET mission: it provides directional fluxes covering the energy range  $18 \div 500$  MeV (Heynderickx et al. 1999). Data were derived by using the SPENVIS web-tool (Heynderickx et al. 2000). Both models were constructed following McIlwain’s original procedure with standardized dipole moment  $M_d = 0.311653 G \cdot R_E^3$  independently of epoch (McIlwain 1966).

PAMELA results extend the observational range for trapped protons down to  $L \sim 1.1 R_E$ , and up to the maximum proton kinetic energies corresponding to trapping limits (critical energies  $\lesssim 4$  GeV). Reported vertical bars account only for statistical errors; the total PAMELA systematic uncertainty amounts to  $10 \div 20$  %, decreasing with increasing energy. UP8 predictions deviates from PAMELA points almost everywhere, overestimating fluxes by about one order of magnitude. Instead, a better agreement can be observed between PAMELA and PSB97 predictions. While pitch angle dependencies (Figure 4, middle panels) appear to be consistent, significant deviations from models can be noted between energy spectra (Figure 4, top panels), in fact PAMELA fluxes do not show the structures present in the PSB97 predictions, resulting in a disagreement which amounts up to an order of magnitude at highest energies. Discrepancies in radial shapes at highest  $L$ -shell bins (Figure 4, bottom panels) are due to the limited data resolution at highest spacecraft altitudes, which affects the PAMELA flux intensity estimate.

Finally, Figure 5 shows the comparison between PAMELA results and a theoretical calculation by Selesnick et al. (2007) for the year 2000. Differential fluxes are reported as a function of the first adiabatic invariant  $M$ , for sample values of  $K$  and  $L^*$  invariants (equatorial region). While spectral shapes are in a good qualitative agreement, measured flux intensities result to be up to about an order of magnitude lower with respect to model predictions, depending on the phase-space region.



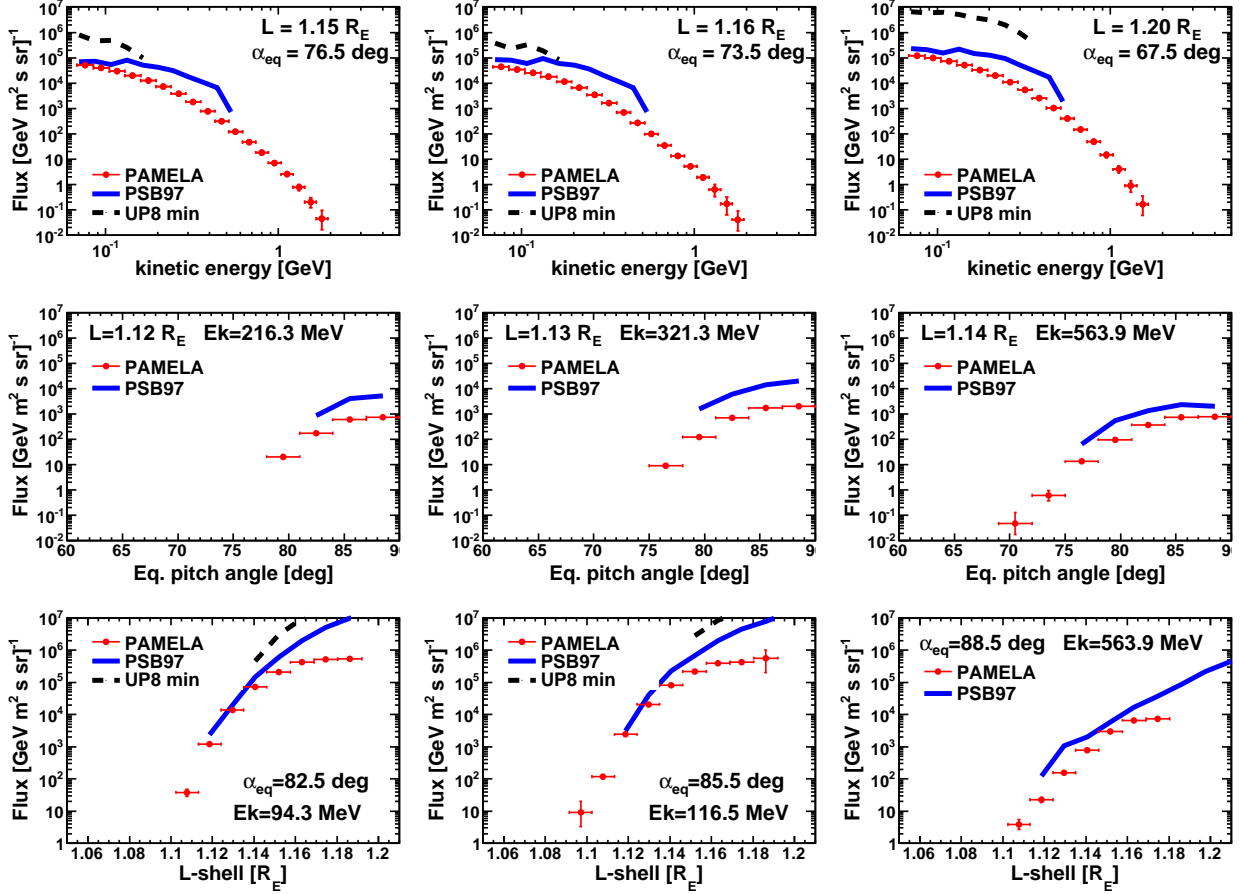


Fig. 4.— Trapped proton energy spectra (top panels), pitch angle profiles (middle panels) and  $L$ -shell profiles (bottom panels) compared with predictions from AP8-min model (Sawyer & Vette 1976) adapted for unidirectional fluxes (UP8-min) and from PSB97 (Heynderickx et al. 1999) model, denoted with dashed black and solid blue lines respectively. Model data are from the SPENVIS web-tool (Heynderickx et al. 2000). Comparisons are reported for combinations of sample  $E_k$ ,  $\alpha_{eq}$  and  $L$ -shell values.

#### 4. Conclusions

PAMELA measurement of energetic ( $\gtrsim 70$  MeV) geomagnetically trapped proton fluxes at low Earth orbits (350÷610 km) have been presented. The analyzed sample corresponds

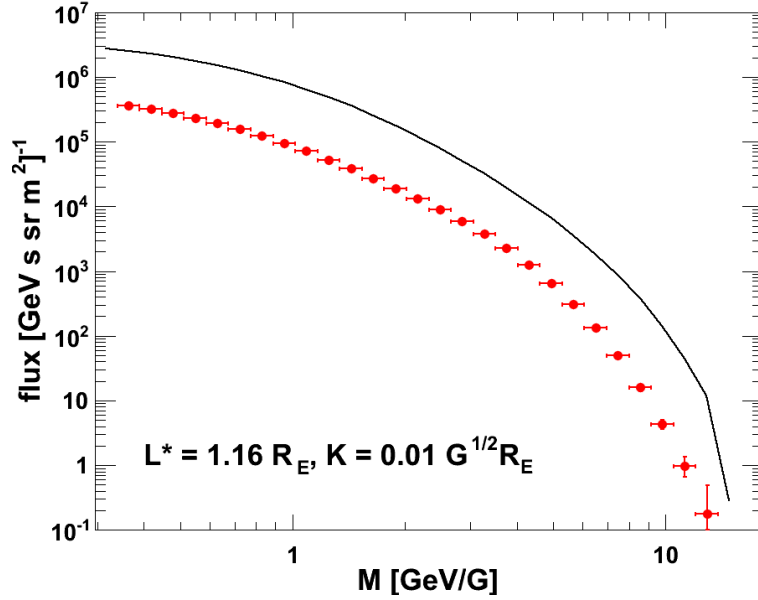


Fig. 5.— Stably-trapped differential flux ( $GeV^{-1}m^{-2}s^{-1}sr^{-1}$ ) at geomagnetic equator compared with a theoretical calculation by Selesnick et al. (2007) for the year 2000. Spectra are reported as a function of first adiabatic invariant  $M$ , for sample values of  $K$  and  $L^*$  invariants.

to data acquired by PAMELA between July 2006 and September 2009. Trajectories of selected events were reconstructed in the magnetosphere by means of a tracing code based on the numerical integration of particle motion equations in the geomagnetic field, and investigated in the framework of the adiabatic theory.

Stably-trapped protons were detected in the South Atlantic Anomaly region, where the inner Van Allen belt makes its closest approach to the Earth’s surface. Measured spectra were compared with predictions of empirical and theoretical models available in the same energy and altitude ranges. PAMELA results extends the observational range for the trapped radiation down to lower  $L$ -shells ( $\sim 1.1 R_E$ ) and up to highest kinetic energies ( $\lesssim 4$  GeV), significantly improving the description of the low altitude radiation environment where current models suffer from the largest uncertainties.

## **Acknowledgements**

We gratefully thank R. Selesnick for helpful discussions, and D. Smart, P. A. Shea and J. F. Cooper for their assistance and support in adapting their trajectory program (Smart & Shea 2000). We acknowledge support from The Italian Space Agency (ASI), Deutsches Zentrum für Luftund Raumfahrt (DLR), The Swedish National Space Board, The Swedish Research Council, The Russian Space Agency (Roscosmos) and The Russian Scientific Foundation.

## REFERENCES

- Adriani, O., Barbarino, G. C., Bazilevskaya, G. A., et al., 2011a, *ApJ* 737 L29.
- Adriani, O., Barbarino, G. C., Bazilevskaya, G. A., et al., *Scienceexpress*, 3 March 2011b.
- Adriani, O., Barbarino, G. C., Bazilevskaya, G. A., et al., 2013, *ApJ* 765:91.
- Boscher, D., S. Bourdarie, P. O'Brien, and T. Guild, *International Radiation Belt Environment Modeling (IRBEM)*, 2012. Available at <http://sourceforge.net/projects/sirbem>.
- Daly, E. J., & Evans, H. D. R., *Rad. Meas.*, vol. 26, no. 3, pp. 363-368, 1996.
- Farley, T. A., & Walt, M., 1971, *J. Geophys. Res.*, 76, 8223–8240.
- Getselev, I. V., et al., 1991, Preprint MGU-91-37/241.
- Gussenhoven, M. S., et al., 1993, *IEEE Trans. Nucl. Sci.*, 40, p. 1450–1457.
- Gussenhoven, M. S., et al., 1995, *IEEE Trans. Nucl. Sci.*.
- Heynderickx, D., Kruglanski, M., Pierrard, V., et al., 1999, *IEEE Trans. Nucl. Sci.*, Vol. 46, pp. 1475–1480.
- Heynderickx, D., Kruglanski, M., Quaghebeur, B., et al., 2002, *SAE Technical Paper* 2000-01-2415.
- Huston, S. L., Kuck, G. A., & Pfitzer, K. A., 1996, *Geophys. Monogr. Ser.*, Vol. 97, pp. 119–122.
- Huston, S. L., & Pfitzer, K. A., 1998, *NASA Contract. Rep.* NASA/CR-1998-208593.
- Lenchek, A. M., & Singer, S. F., 1962, *J. Geophys. Res.*, 67, 4073–4075.
- Looper, M. D., Blake, J. B., Cummings, J. R., et al., 1996, *Radiat. Meas.*, 26(6):967-78.

- Looper, M. D., Blake, J. B., Mewaldt R. A., 1998, *Adv. Space Res.*, 21(12):1679-82.
- Macmillan, S., & Maus, S., *Earth Planets Space*, 57, 11351140, 2006.
- McIlwain, C., 1966, *Space Sci. Rev.* 5, 585-589.
- Meffert, J. D., & Gussenhoven, M. S., 1994, PL-TR-94-2218, *Environ. Res. Pap.* 1158, Air Force Res. Lab., Wright-Patterson Air Force Base, Ohio.
- Picozza, P., Galper, A. M., Castellini, G., et al., 2007, *Astropart. Phys.*, Vol 27, Pages: pp. 296-315.
- Roederer, J., 1970, Springer-Verlag, New York.
- Sawyer, D. M., & Vette, J. I., 1976, NSSDC/WDC-A-R&S 76-06.
- Selesnick, R. S., Cummings, A. C., Cummings, J. R., et al., 1995, *J. Geophys. Res.*, Vol. 100, Issue A6, pp 9503-9518.
- Selesnick, R. S., Looper, M. D., & Mewaldt, R. A., 2007, *Space Weather*, Vol. 5, S04003.
- Singer, S. F., 1958, *Phys. Rev. Lett.*, 1, 181–183.
- Smart, D. F., & Shea, M. A., 2000, Final Report, Grant NAG5-8009, Center for Space Plasmas and Aeronomic Research, The University of Alabama in Huntsville.
- Smart, D. F., & Shea, M. A., 2005, *Adv. Space Res.*, 36, 2012–2020.
- Sullivan, J. D., 1971, *Nucl. Instr. and Meth.* 95, 5.
- Tsyganenko, N. A., & Sitnov, M. I., *J. Geophys. Res.*, Vol. 110, A03208, 2005.
- Walt, M., 1994, *Introduction to Geomagnetically Trapped Radiation*, Cambridge Univ. Press. (New York).

Xapsos, M. A., et al., 2002, IEEE Trans. Nucl. Sci., 49, 2776–2781.